Shear stress-induced Piezo1 activates CD99L2 to facilitate the initiation of blood circulation

Jingao Lu[1,2,4,5], Jun Zhao[1,2,5], Xin Tang[1,2,5], Ente Zhu[1,2], Jin Xu[1,2], Xiaohui Chen[1,2], Qiang Wang[1,2], Zhibin Huang[1,2,6,7****], Ning Ma[3,6***], Wenqing Zhang[1,2,6**], Wei Liu[1,2,6*]

[1] Innovation Centre of Ministry of Education for Development and Diseases, School of Medicine, the Sixth Affiliated Hospital of South China University of Technology (Nanhai District People's Hospital of Foshan), Foshan, 528200, China.

[2] Innovation Centre of Ministry of Education for Development and Diseases, School of Medicine, South China University of Technology, Guangzhou, 510006, China.

[3] GDMPA Key Laboratory of Key Technologies for Cosmetics Safety and Efficacy Evaluation, NMPA Key Laboratory for Safety Evaluation of Cosmetics, Department of Histology and Embryology, School of Basic Medical Sciences, Southern Medical University, Guangzhou 510515, China.

[4] Present address: Xiaogu Wei Street, South China University of Technology, Guangzhou, China.

[5]These authors contributed equally

[6] Senior author

[7] Lead contact

*Correspondence: liuwei7@scut.edu.cn

**Correspondence: mczhangwq@scut.edu.cn

***Correspondence: mn1228@smu.edu.cn

****Correspondence: huangzhb1986@scut.edu.cn

SUMMARY

The onset of blood circulation is a pivotal developmental event, yet the molecular mechanisms that enable erythrocytes to disengage from the endothelium and enter the bloodstream remain unclear. Here, we identify CD99L2 as a mechanoresponsive adhesion regulator, transiently induced in primitive erythrocytes by shear stress–activated Piezo1 signaling. Using zebrafish and mouse models, we show that CD99L2 is essential for erythrocyte de-adhesion and circulation entry. Loss of CD99L2 leads to aberrant nuclear translocation of β-catenin, activation of Rap1 signaling, and persistent expression of adhesion molecules, culminating in erythrocyte retention, impaired maturation, and hemolytic anemia. Mechanistically, CD99L2 binds and anchors β-catenin at the membrane, and shear-induced Piezo1 activation promotes its expression during a narrow developmental window. This pathway is conserved in mice and modulated by biomechanical forces, unveiling a mechanism that couples hemodynamic force to erythrocyte adhesion control during the initiation of blood flow.

KEYWORDS

CD99L2; Piezo1; circulation initiation; erythrocyte adhesion; shear stress; hemolytic anemia

INTRODUCTION

The initiation of blood circulation is a crucial developmental milestone that ensures the delivery of oxygen and nutrients to growing tissues, and provides essential mechanical and chemical cues for vascular morphogenesis and remodeling[1,2]. This complex process involves coordinated events including vessel lumen formation, heartbeat onset, integration of erythrocytes into the bloodstream, and importantly, the timely detachment of erythrocytes from the vascular endothelium[3,4,5]. In mouse embryos, primitive erythroblasts and the nascent vascular plexus emerge around embryonic day (E) 7.5, followed by heartbeat initiation at E8.0 and the onset of erythroblast circulation at approximately E8.5, coinciding with the 5-somite stage[6,7,8]. During this period, erythroid precursors transiently adhere to the vascular lumen after invading from the subaortic region, before being synchronously released into circulation[9]. Following circulation establishment, hemodynamic forces such as shear stress and circumferential stretch drive vascular remodeling alongside chemical signals like hypoxia and nutrient demands[10,11].

Traditionally regarded as passive oxygen carriers, emerging evidence indicates that erythrocytes actively regulate their adhesion to endothelial cells to facilitate their entry into circulation. Zebrafish studies revealed that prior to flow initiation, erythrocytes form vinculin-enriched membrane protrusions towards endothelial

cells, suggesting dynamic adhesive interactions[3]. Persistent adhesion, however, can impede erythrocyte release, with metalloproteinases proposed to facilitate detachment, though the precise molecular mechanisms governing erythrocyte de-adhesion remain largely unknown. Notably, mouse embryonic data suggest that loss of adhesion is a prerequisite for the onset of blood flow rather than a downstream consequence[5].

Adhesion molecules classically involved in leukocyte trafficking also contribute to erythropoiesis and erythrocyte localization. For instance, platelet-endothelial cell adhesion molecule-1 (PECAM-1) participates in primitive erythrocyte differentiation and vascular association[12,13,14,15] [12-15]. Under physiological conditions, mature erythrocytes exhibit minimal adhesion; however, pathological adhesion contributes to vascular complications in diseases such as diabetes and malaria by promoting erythrocyte-endothelial interactions that trigger thrombosis and vaso-occlusion[16,17]. A major feature of sickle cell anemia disease (SCD) is the significantly increased adhesion of blood cells[18]. Studies have found that Piezo1 activation reduces the deformability of sickle RBCs and increases their tendency to sickle and adhere to laminin under hypoxic conditions. This is related to the activation of the Gárdos channel and Ca^{2+} influx[19]. This evidence also confirms the regulatory role of Piezo1 activation and Ca^{2+} influx on the adhesion status of red blood cells.

Here, we uncover a role for the adhesion molecule CD99L2 in orchestrating the initiation of blood circulation via modulation of erythrocyte-endothelial adhesion. While CD99L2 was previously characterized for its function in neutrophil trans-endothelial migration, our analysis of mouse single-cell RNA sequencing data reveals its specific and transient expression in primitive erythroid progenitors, temporally aligned with circulation onset. Functional experiments in zebrafish demonstrate that knockdown of *cd99l2* disrupts erythrocyte release into the bloodstream, a phenotype recapitulated in mouse mutants. Transcriptomic profiling of erythrocytes deficient in *cd99l2* highlights upregulation of adhesion molecules and activation of Rap1 signaling coupled with aberrant nuclear translocation of β-catenin.

Importantly, we identify that shear stress generated by heartbeat activates the mechanosensitive ion channel Piezo1 in erythrocytes, which in turn induces *CD99L2* gene expression within a critical developmental window. This mechanotransduction pathway links biomechanical forces to molecular control of erythrocyte adhesion and circulation initiation. Our findings illuminate an axis—Piezo1-mediated mechanosensing regulates CD99L2 to facilitate erythrocyte de-adhesion and blood flow onset—offering new insights into hematopoiesis and potential therapeutic targets for erythroid and vascular disorders.

RESULTS

CD99l2 is specifically expressed in erythrocytes during the initiation of blood flow

In order to find the adhesion molecules that play a key function during the initiation of circulation, we utilized a single-cell RNA-sequencing data to screen the expression of various adhesion molecules in early embryonic development in mice[20]. We compared multiple molecules involved in leukocyte deadhesion, adhesion molecules on erythrocyte membranes, and multiple molecules that regulate erythrocyte adhesion in pathological situations[21,22], we found that the expression level of *CD99l2* in early embryonic erythrocytes of mice is significantly elevated compared to other adhesion molecules, and the expression trend is consistent with the initiation of blood flow in mouse red blood cells (Figures 1A-B). *CD99l2* began to be expressed in mouse erythrocytes at E7.75, peaked at E8.25, and then began to decrease. This specific expression window coincides with the entry of mouse erythrocytes into the circulation[23]. Previous studies in mice have identified CD99l2 as an adhesion factor that is expressed on vascular endothelial cells and leukocytes and mediates leukocyte trans-endothelial migration and adhesion[24,25]. Furthermore, we found that *CD99l2* was significantly enriched in the cluster of committed erythroid progenitor cells (CMPs) compared to other known erythrocyte surface adhesion genes including *Cd44*, *Cd47*, *Cd108*, *Cd151*, and *Cd49d* (Figure S1A) [26,27]. These results indicate that CD99l2 may play a key role in the early development of mouse erythrocytes.

Since observing early embryonic cell development or the initiation of blood circulation in real-time in mammals is challenging, we have chosen zebrafish as the model organism for further research. We observed a significant process of de-adhesion of erythrocytes before they enter the blood flow (Figure S1B). Whole-mount in situ hybridization (WISH) was used to examine the spatiotemporal expression pattern of

the *cd99l2* gene in zebrafish. We found that *cd99l2* mRNA was expressed in the intermediate cell mass (ICM) at 22 hpf (hours post fertilization) (Figure 1C), followed by expression in the yolk at 26 hpf (Figures 1E-E'). A gradual decline in *cd99l2* expression was observed in the ICM after 30 hpf (Figures 1 F-F'). At 32 hpf, minimal *cd99l2* expression was observed in the ICM (Figures 1G-G'). Since zebrafish initiate heartbeat and subsequent circulation around 24 hpf [1,4,28], our findings suggest that *cd99l2* may have a potential role in this process (Figure1 H).

We used a double labeling technique that combined WISH to detect *cd99l2* mRNA expression with immunostaining for Hbae1.1 protein, an erythrocyte marker, to determine which cell types expressed *cd99l2* at 26 hpf. We found that Hbae1.1+ cells co-localized with *cd99l2*$^{+}$ cells within the ICM and yolk regions (Figures 1I and S1C-F), confirming that *cd99l2* is expressed in erythrocytes. Next, we quantitatively compared *cd99l2* mRNA expression levels across different hematopoietic lineages in cell populations isolated from transgenic zebrafish at 28 hpf (primitive hematopoiesis), and at 6 and 7 dpf (days post fertilization) (definitive hematopoiesis). Cell populations were sorted by flow cytometry using specific transgenic markers including *fli1a* for vascular cells, *coronin1a* for myeloid cells, globin for erythroid cells, and *rag2* for lymphoid cells (Figures S1G-H). qRT-PCR analysis revealed that *cd99l2* expression levels were the highest in globin:DsRed-positive cells at 28 hpf (Figure S1I), suggesting that *cd99l2* expression is associated with primitive rather than definitive erythropoiesis. The Western Blot confirmed this result on protein level (Figures S1J-K). Next, we developed a reporter line that enabled dynamic monitoring of *cd99l2* expression to further characterize the expression pattern of *cd99l2* and facilitate future studies. We created the transgenic construct Tg (*cd99l2*: eGFP) by isolating a 4.7-kb DNA fragment upstream of the *cd99l2* translation start site to drive GFP expression. Co-staining of the reporter with *gata1*: DsRed, an erythroid precursor marker, revealed that *cd99l2*: eGFP expression overlapped with the expression of *gata1*$^{+}$ erythroid precursors both spatially and temporally in the ICM and yolk (Figures S1L-M), indicating that *cd99l2*: eGFP was specifically expressed on erythroid progenitors. Further characterization of the Tg(*cd99l2*: eGFP) transgenic zebrafish validated the fidelity of the transgenic model, with *cd99l2*: eGFP expression patterns consistent with endogenous *cd99l2* expression patterns detected by WISH (Figure 1J). May–Grünwald Giemsa staining of peripheral blood from Tg(*cd99l2*: eGFP) zebrafish confirmed that these cells were erythrocyte precursors (Figure 1K). To better validate this finding at the protein level, we constructed the *cd99l2* promoter: Cd99l2 CDS-eGFP plasmid. By observing fluorescence, we found that the Cd99l2 protein also exhibited a brief, specific temporal expression window on erythrocytes (Figures S1N-O).

Taken together, our results reveal that CD99l2 is specifically expressed in erythrocytes during the initiation of blood flow in both mouse and zebrafish.

cd99l2 has a critical role in the onset of circulation

Since our results demonstrated that *cd99l2* was transiently expressed in primitive erythroid progenitors (18 hpf-32 hpf), we next sought to determine the role of *cd99l2* in early erythropoiesis. To assess the function of *cd99l2* in zebrafish, we designed an antisense morpholino oligonucleotide (MO) targeting the translation initiation site and evaluated its efficiency (Figures S2A-B). At 28 hpf, despite established blood circulation, *cd99l2*-deficient morphants exhibited restricted β-globin exon-1 (βe1) expression in the trunk, with no signal detected in the heart and head regions (Figures 2A-B). This phenotype persisted beyond 2 dpf (Figures S2C-D). Exogenous overexpression of *cd99l2* mRNA or driving *cd99l2* expression under the control of the *gata1* promoter rescued the phenotype in *cd99l2*-deficient morphants, suggesting that erythrocyte stagnation is a consequence of *cd99l2* deficiency (Figures 2C-D). Importantly, no abnormalities were observed in other blood cell lineages, suggesting that *cd99l2* knockdown specifically affected erythrocytes (Figures S2E-J). To determine the significance of the timing of *cd99l2* expression, we developed a heat-shock inducible system (hsp70l:*cd99l2*-eGFP). We found that heat-shock-induced *cd99l2* overexpression at 24 hpf rescued the erythrocyte phenotype in *cd99l2*-deficient morphants, while overexpression at 32 hpf did not (Figures 2F-G). These findings highlighted the critical function of *cd99l2* prior to the onset of circulation.

To explore all potential causes of the observed phenotype, we next examined various factors that are crucial for blood flow initiation in MO embryos including the onset of erythroid progenitor production, heart contraction, vessel integrity and plasma flow, and erythrocyte entry into and release from circulation[5]. *gata1*$^{+}$

erythroid progenitor production appeared normal at 24 hpf in *cd99l2*-deficient morphants (Figure S2K-L). Furthermore, no apparent effects were observed on the heartbeat (Figure S2M), *fli1a*: eGFP^{+}-labeled blood vessel development, or plasma flow monitored by injection with fluorescent dextran (Figure 2H). A parabiosis experiment showed that *gata1*$^{+}$ red blood cells from control embryos flowed through the vasculature network to the distal region of *cd99l2*-deficient morphants (Figures 2I-I'), indicating vascular patency. Living imaging of Tg(globin: DsRed) and Tg(*fli1a*: eGFP) double-transgenic embryos was used to monitor erythrocyte behavior. We found that in *cd99l2*-deficient morphants globin^{+} cells migrated into the vessel but remained stuck within *fli1a*$^{+}$ cells, indicating failed detachment from vessel walls and segregation from each other before synchronous release into circulation (Figures 2J-K). Using transmission electron microscopy to examine the position of erythrocytes within the vessels, we found significant disconnection of erythrocytes from the vessel walls in control embryos but not in *cd99l2*-deficient morphants during the initiation of blood flow, and the morphology of erythrocytes is significantly abnormal in *cd99l2*-deficient morphants (Figures 2L-O). These results indicate that *cd99l2* is indispensable for initiation of blood flow in zebrafish.

To investigate the functional role of *cd99l2*, we established a *cd99l2* mutant zebrafish model using TALEN technology (Figure S2N). In situ hybridization analysis revealed the absence of phenotypes consistent with transient *cd99l2* knockdown in the mutant zebrafish (Figure S2O). This discrepancy could potentially be attributed to genetic compensation effects commonly observed in zebrafish gene mutants, which often mask the phenotypic manifestations seen in transient knockdown models[29,30]. To test this hypothesis, we inhibited genetic compensation through *upf3a* morpholino (MO) injection. Remarkably, blocking genetic compensation in *cd99l2* mutants restored the phenotype consistent with transient knockdown (Figure S2P). Furthermore, transient knockout of *cd99l2* using the CRISPR-Cas9 system recapitulated the phenotype observed in morpholino-mediated knockdown experiments (Figures S2Q-T).

Disruption of *cd99l2* leads to erythrocyte maturation defects and hemolytic anemia in zebrafish

As we mentioned above, we observed a significant change in erythrocyte morphology following the deletion of *cd99l2*. In order to confirm this result, we further examined the cytological defects in erythrocytes using flow cytometry to sort *gata1*: DsRed-labeled erythroid cells. We found a marked decrease in fluorescent cell counts in *cd99l2*-deficient morphants at 28 hpf. Giemsa staining revealed arrested differentiation at the basophilic erythroblast stage, characterized by abnormal membrane morphology (Figures 3A-B). Moreover, a notable increase in the ratio of binucleated cells was observed in *cd99l2*-deficient morphants (Figure 3C). The maturation of erythrocytes requires access to blood flow. We found a significant reduction in *alas2*, a marker of mature erythrocytes, expression levels in *cd99l2*-deficient morphants (Figures 3D-E, H), as well as compromised hemoglobin activity (Figures 3F-G, I). These findings indicated that erythrocyte maturation was impaired following *cd99l2* knockdown. In addition, an osmotic fragility test indicated changes in the tolerance to osmotic-induced stress in *cd99l2*-deficient morphants (Figures 3J-K). TUNEL staining revealed increased apoptosis in erythrocytes following the knockdown of *cd99l2* (Figures 3L-M). Together, our findings suggest the onset of severe hemolytic anemia in *cd99l2*-deficient morphants.

Abnormal erythropoiesis in zebrafish is caused by activation of the Rap1 signaling pathway and the translocation of β-catenin

To elucidate the specific regulatory mechanisms underlying *cd99l2* knockdown-induced abnormal erythropoiesis, we performed RNAseq analysis on erythrocytes sorted from both Control MO and *cd99l2* MO groups. We observed 666 up genes and 488 down genes between Control MO and *cd99l2* MO groups (Figure S3A). Enrichment analysis of the KEGG pathway revealed a significant enrichment of the leukocyte trans-endothelial migration pathway, as previously studied in the context of *cd99l2* function. In addition, we observed enrichment of the Rap1 signaling pathway (Figure 4A). Analysis of pathway-related gene expression also demonstrated indicative of Rap1 signaling pathway activation following *cd99l2* knockdown (Figure 4B). The Rap1 signaling pathway has been implicated in various cellular processes, including cell adhesion and junction regulation, cell migration, polarization, proliferation, and survival[31,32]. We next sought to determine the role of the Rap1 signaling pathway in erythrocyte behavior by disrupting its activity in *cd99l2*-deficient embryos. Knockdown of Rap1a via injection of Cas9 protein and *rap1a* guide RNA

prevented activation of the Rap1 signaling pathway and restored normal erythrocyte flow into the bloodstream, but *rap1b* CRISPREN did not work (Figures 4C, E and Figures S3B-C). Rap1 GTPases are ubiquitously expressed binary switches that alternate between active and inactive states and are regulated by diverse families of guanine nucleotide exchange factors (GEFs) and GTPase-activating proteins (GAPs). Conversely, overexpression of *rapgef4* led to defective erythropoiesis in wildtype zebrafish but not *rapgef5b* (Figures 4D, F and Figures S3D-E).

The RNAseq analysis revealed a significant upregulation in the expression of various cell adhesion molecules (CAMs) (Figure S4F). Real-time PCR yielded the same results (Figure S4G). Among these, extensive screening using WISH revealed that *cdh15* and *jam2a* expression levels were significantly increased prior to the onset of circulation (Figure S4H). Notably, following initiation of circulation, the expression levels of *cdh15* and *jam2a* were not significantly decreased in *cd99l2*-deficient embryos, unlike other CAMs which showed no significant temporal changes. Given the persistence of *cdh15* and *jam2a* expression in *cd99l2* MO embryos, we next investigated the underlying mechanisms driving this anomaly. Previous studies have linked the nuclear localization of free β-catenin caused the abnormal adhesion[33]. Here, our immunostaining analysis revealed abnormal nuclear localization of β-catenin in erythrocytes following *cd99l2* knockdown (Figure 4G). Further studies using inhibitors that block the nuclear entry of β-catenin restored normal blood flow (Figure 4H).

It is reported that the activation of Rap1 was mediated via β-catenin and RapGEF2 when adhere junctions (AJs) was disrupted[34]. Further studies using inhibitors that block the nuclear entry of β-catenin not only restored normal blood flow but also significantly decreased the expression levels of Rap1-related guanine exchange factors (Figure 4I). The results of CHIP-PCR demonstrated that the β-catenin/TCF3 and β-catenin/TCF4 complex had a binding site on the promoter of *rapgef4* which could activate its transcription (Figure 4J). The deficiency of Cd99l2 leads to the release of stable β-catenin into the nucleus, which in turn activates the RAP1 signaling pathway. To verify our inference, we have performed a series of verifications on the combination of *cd99l2* and β-catenin. We found that *cd99l2* expressed co-localized with β-catenin on cell membrane in erythrocytes (Figure 4K). Co-IP further confirms the binding between *cd99l2* and β-catenin (Figure 4L). As a transmembrane protein, Cd99l2 is divided into intracellular, transmembrane and extracellular regions. We found that the binding of *cd99l2* and β-catenin disappeared through deleting the intracellular region of *cd99l2* (Figure 4N). Furthermore, we predicted the specific binding site of *cd99l2* and β-catenin by alphafold2 (Figures 4M, S4I-J). The binding of *cd99l2* and β-catenin was disappeared after mutating the predicted binding sites (Figure 4N). Our comprehensive analysis highlights the critical role of β-catenin in modulating erythrocyte adhesion through activating the Rap1 signaling pathway in *cd99l2*-deficient zebrafish.

The activation of Piezo1 and calcium channels induces the expression of *cd99l2*

The shear stress generated by the heartbeat is crucial for initiating blood circulation. To investigate whether this shear stress regulates the specific expression of Cd99l2, we simulated and indicated the generation of shear stress by injecting dextran into the heart of the zebrafish. Before the heartbeat (22 hpf), we injected fluorescently labeled dextran at the site of the heart. After the shear stress generated by the beating heart, the fluorescently labeled dextran gradually diffuses throughout the circulatory system of the zebrafish. Using this approach, we found no significant changes in the number or distribution of *gata1* labeled cells before and after the onset of the heart beat (Figure S4A). However, we have observed that when dextran reaches the whole body through the heart, the expression of *cd99l2* is significantly elevated (Figures 5A-B). This observation suggests that *cd99l2* expression is upregulated in response to the shear stress generated by heartbeats. In order to validate our hypothesis, we employed the cardiac development inhibitor Blebbistatin for verification. After treatment, the development of the zebrafish heart was impaired, preventing the beating of heart, and we observed the unsuccessful initiation of blood flow (Figure S4B). Consistent with our hypothesis, *cd99l2* expression was significantly reduced upon heartbeat inhibition, confirming that shear stress is essential for its induction (Figures 5C-D).

Piezo1 is a common mechanosensor for shear stress on the cell membrane. Shear stress from blood flow can activate Piezo1 on the vascular endothelium, assisting endothelial cells in anchoring to complete vascular remodeling[35]. Furthermore, when passing through narrow blood vessels, the shear stress exerted by blood flow activates Piezo1 channels on erythrocytes, leading to Piezo1-mediated Ca^{2+} influx. This

results in K^+ efflux and water loss, leading to a temporary decrease in cell volume, which aids in their passage through the vessels[36]. In order to investigate whether Piezo1 and Ca^{2+} channels are involved in the regulation of *cd99l2* by shear stress, we used the calcium indicator GCaMP6s and created Tg (*gata1*: GCaMP6s) transgenic zebrafish to observe the activation of calcium signaling during the initiation of circulation. Imaging observations showed that when erythrocytes begin to form at 20 hpf, GCaMP6 signals have already started to be expressed. By 22 hpf, as red blood cell expression gradually increases, GCaMP6 signals also gradually increase. At 24 hpf, when blood flow begins to start, GCaMP6 signals start to decrease, and by 26 hpf, after the onset of blood flow, GCaMP6 expression is almost gone (Figure S4C). These results indicate a transient calcium signal in erythrocytes surrounding the onset of blood flow. Notably, this calcium signal window (20–24 hpf) precedes the cd99l2 expression window (24–28 hpf) (Figure S4D), positioning calcium as a potential upstream trigger. Furthermore, we utilized the common Piezo1 inhibitor GsTMx4 and activator Yoda1. After treatment, we observed a significant change of the expression of *cd99l2* in zebrafish (Figures 5E-H). To genetically validate Piezo1's role, we performed erythrocyte-specific knockout of *piezo1*. This cell-autonomous ablation prevented blood flow initiation (Figures 5I, K), confirming its critical role. The results showed that when *piezo1* expression in red blood cells was abnormal, zebrafish could not normally initiate blood flow, indicating that it plays a key role in the initiation of circulation. To further confirm the way Piezo1 regulates *cd99l2* expression, we screened using inhibitors on the classic downstream pathways of Piezo1, and ultimately demonstrated that inhibition of the Erk1/2 pathway resulted in blood flow stasis in zebrafish (Figures 5J, L, S4E). Previous studies have shown that the Piezo1 / ERK1/2 signaling axis plays a key role in the early differentiation of erythrocytes[37]. Further experiments demonstrated that when *piezo1* is absent and the ERK1/2 signaling pathway is inhibited, *cd99l2* expression is significantly reduced (Figures 5M-N).

Together, Together, these results establish that shear stress, sensed by Piezo1 and transduced via calcium influx and the ERK1/2 pathway, is crucial for both the initiation of blood flow and the induction of *cd99l2* expression.

Conservation validation of the roles of CD99L2, PIEZO1, and calcium activation in the initiation of blood flow

To study the functional conservation of CD99L2, we constructed CD99l2 knockout mice. We found that erythrocytes were eliminated in the yolk sac of Cd99l2 knockout mice at E8.5 despite the presence of vessels (Figures 6A-B). H&E staining of CD99l2 knockout mice also revealed the phenomenon of erythrocytes clogging in blood vessels (Figures 6C-D). Immuno-fluorescence staining was performed on slices of mouse embryos, we observed the nuclear translocation of β-catenin in the CD99l2 Knock-out erythrocytes, which was consistent with the phenotype we observed in zebrafish (Figures 6E-H). The expression level of Jam2 was also significantly increased in mutant mice, consistent with the zebrafish phenotype (Figures 6I-K). Furthermore, knockdown of *CD99L2* in U2-OS cells induced abnormal nuclear localization of β-catenin (Figures 6L-M). The mRNA expression level of JAM2 and CDH15 were also elevated (Figure 6N). In addition to the functional conservation of CD99L2, we also verified the activation of Piezo1 and calcium channels by shear stress. To apply a defined shear stress *in vitro*, we utilized flow cytometry cell sorting, a process known to exert mechanical pressure on cells [38]. Subjecting K562 cells to this procedure induced a significant increase in Fluo-4 calcium signal (Figures 6O-P), confirming mechanical activation. Further immunofluorescence experiments showed that CD99L2 expression was significantly increased in sorted K562 cells, and qPCR experiments further confirmed this result (Figures 6Q-S). These results demonstrate that shear stress activates a conserved Piezo1-calcium signaling axis to regulate CD99L2 expression across species.

DISCUSSION

The initiation of blood circulation is a pivotal but mechanistically intricate event in vertebrate development. Our study identifies CD99L2 as a critical regulator of this process, operating at the interface of mechanotransduction and intercellular adhesion. We demonstrate that CD99L2 exhibits a stage-specific expression pattern in primitive erythrocytes and is essential for their maturation and timely entry into

circulation. Disruption of CD99L2 leads to erythrocyte retention, hemolytic anemia, and a complete failure to establish blood flow, underscoring its indispensable role.

A central mechanistic finding is the reciprocal regulation between CD99L2 and the β-catenin/Rap1 adhesion axis. CD99L2 deficiency causes aberrant nuclear accumulation of β-catenin, which hyperactivates Rap1 signaling, thereby stabilizing erythrocyte-endothelial adhesions. This positions CD99L2 as an upstream negative regulator of a conserved adhesion module, revealing a checkpoint that must be disengaged for circulation to commence.

Furthermore, we delineate the upstream trigger for CD99L2 expression: hemodynamic force. We provide multi-layered evidence that the shear stress generated by the first heartbeats is sensed by the mechanosensitive ion channel Piezo1 on erythrocytes. This activation triggers a calcium- and ERK1/2-dependent signaling cascade that precisely upregulates cd99l2 transcription within a narrow developmental window. This establishes a direct mechano-chemical pathway (Shear Stress → Piezo1 → Ca^{2+} → ERK1/2 → CD99L2) that translates a physical stimulus into a transcriptional program for de-adhesion.

Collectively, our data support a model in which CD99L2 acts as a shear stress-responsive disengagement signal, coupling cardiac function to the release of erythrocytes into circulation (Figure 7). In this model, nascent erythrocytes are initially anchored to the vascular niche. The onset of heartbeat-generated shear stress is sensed by erythrocyte Piezo1, triggering a calcium-ERK1/2-CD99L2 activation cascade. The induced CD99L2 then functions to antagonize the β-catenin/Rap1-mediated adhesion program, thereby licensing erythrocyte detachment. This creates a positive feedback loop: the initial weak flow promotes the release of more cells, which in turn increases and stabilizes circulation.

This mechanism identifies a mechanosensitive checkpoint in developmental hematopoiesis. It positions CD99L2 not merely as an adhesion molecule, but as a bidirectional regulator that transduces a physical force into a biochemical signal to actively dismantle adhesive contacts—a paradigm that may extend to other progenitor niche exit events. The delineated pathway provides a comprehensive molecular framework for understanding the mechanobiology of circulatory onset.

Limitations of the study

Our study has several limitations. First, while we focused on the adhesion defect as the primary cause of circulation failure, the concomitant cytoskeletal and cell division abnormalities in *cd99l2* mutants were not fully dissected. Determining whether these are direct or secondary consequences links CD99L2 to broader aspects of erythrocyte maturation and membrane integrity. Second, the immediate transcriptional regulators downstream of ERK1/2 that bind the *cd99l2* promoter remain to be identified, representing a key node for deeper mechanistic understanding. Furthermore, the role of endothelial cells in the initiation of blood flow should not be overlooked. Particularly, previous studies have shown that Piezo1 expressed on endothelial cells serves as an important sensor of blood flow and is involved in regulating the adhesive state of these cells. Investigating the role of endothelial cells in the initiation of blood flow will be one of the directions of our future research. Finally, the translational relevance of this pathway in human pathophysiology requires further investigation. It will be important to examine whether dysregulation of the Piezo1-ERK1/2-CD99L2 axis contributes to erythrocyte adhesion disorders in humans, such as congenital dyserythropoietic anemia (CDA) or sickle cell disease (SCD), where aberrant cell-cell interactions and mechanosensitivity are known pathological features.

RESOURCE AVAILABILITY

Lead contact

Requests for further information and resources should be directed to and will be fulfilled by the lead contact, Zhibin Huang (huangzhb1986@scut.edu.cn.)

Materials availability

All unique/stable reagents generated in this study are available from the lead contact with a completed materials transfer agreement. The RNA-seq data has been publicly available by the accession number of PRJNA1426740 on NCBI.

Data and code availability

- Data reported in this paper will be shared by the lead contact upon request.
- This paper does not report original code.
- Any additional information required to reanalyze the data reported in this paper is available from the lead contact upon request.

ACKNOWLEDGMENTS

This work was supported by the National Key R&D Program of China (2024YFA1802200, 2023YFA1800100), National Natural Science Foundation of China (32570966, 32170830), Guangdong Basic and Applied Basic Research Foundation (2024B1515040019), Natural Science Foundation of Guangdong Province, China (2021A1515010422), and Fundamental Research Funds for the Central Universities (2022ZYGXZR031)

AUTHOR CONTRIBUTIONS

J.A.L. and J.Z, X.T designed and did most of the experiments; E.T.Z. analyzed data; J.A.L., N.M. and Z.B.H designed experiments, interpreted data, and wrote the manuscript; W.L., N.M., W.Q.Z., and Z.B.H discussed the results and provided critical advice.

DECLARATION OF INTERESTS

The authors declare that they have no competing interests.

SUPPLEMENTAL INFORMATION

Document S1. Figures S1–S6

Video S1. Living image of GcaMp6s in erythrocytes, related to Figure 5

FIGURE TITLES AND LEGENDS

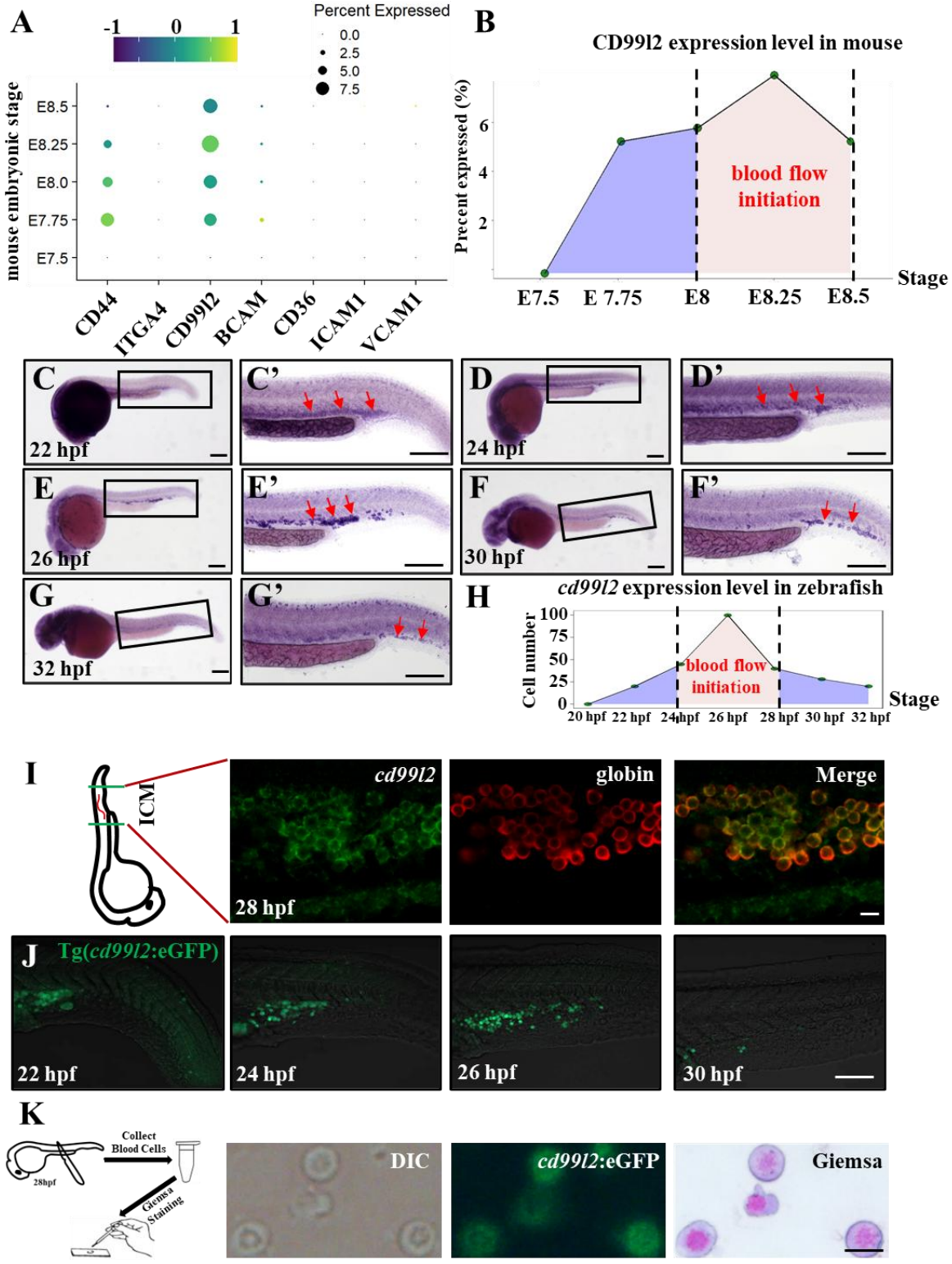

FIGURE 1. CD99L2 IS SPECIFICALLY EXPRESSED IN ERYTHROCYTES DURING THE INITIATION OF BLOOD FLOW

(A) Various of adhesion molecules on mouse erythrocytes based on mouse embryonic single-cell data analysis.

(B) Expression level of Cd99l2 on mouse erythrocytes.

(C-G) WISH was used to examine the expression pattern of the cd99l2 gene during zebrafish embryogenesis.

(H) Expression level of *cd99l2* on zebrafish erythrocytes.

(I) Colocalization of WISH-labeled *cd99l2*: eGFP and globin: DsRed in zebrafish.

(J) Expression pattern of Tg(*cd99l2*: eGFP) during zebrafish embryogenesis.

(K) Representative images showing Giemsa staining of Tg(*cd99l2*: eGFP) positive cells.

Scale bar: 10 μm (I, K) and 100 μm (C-F, J).

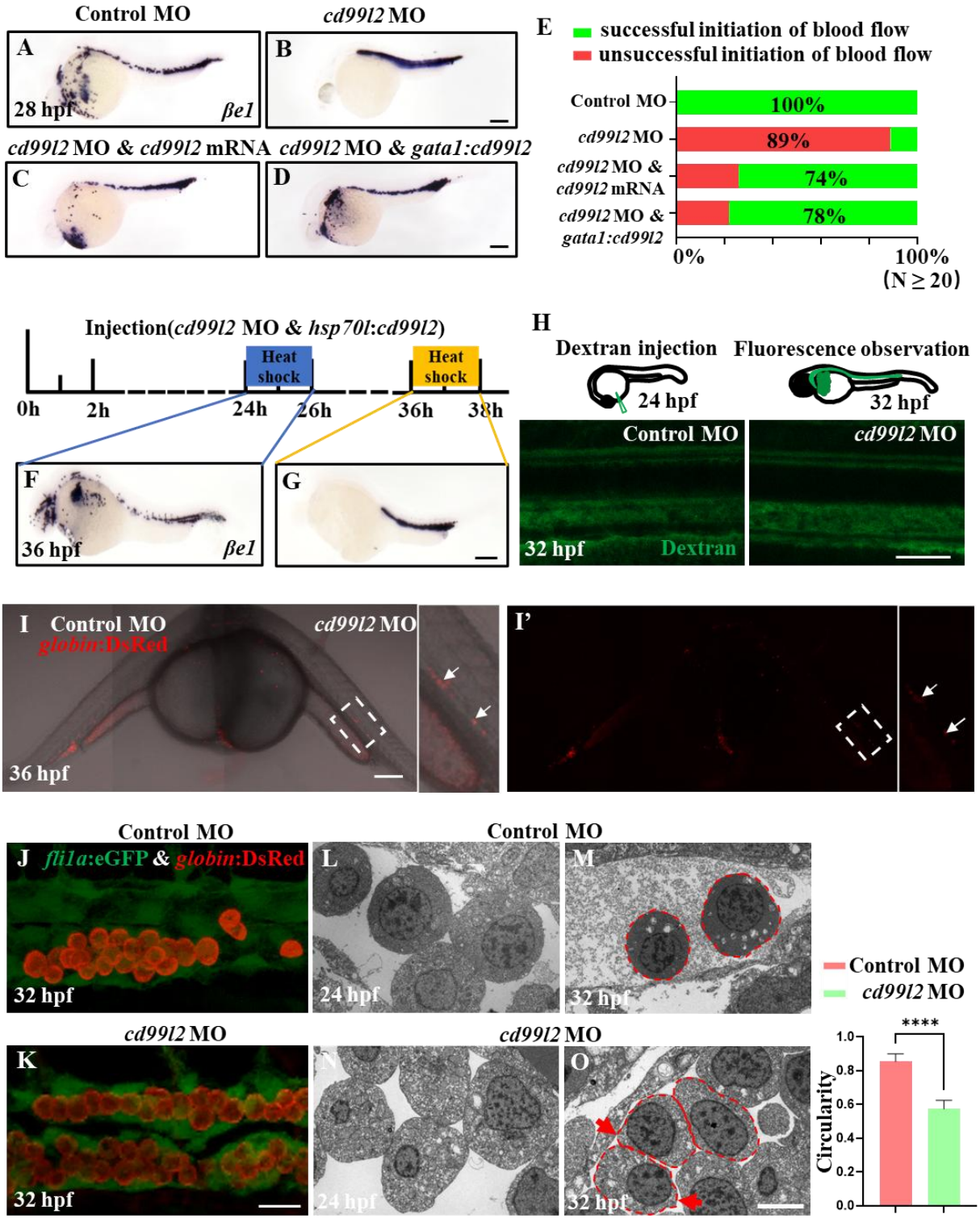

401

402 **FIGURE 2. CD99L2 HAS A CRITICAL ROLE IN THE ONSET OF CIRCULATION**

403 (A-B) WISH was used to detect *βe1* expression in Control MO and *cd99l2* MO erythrocytes.

404 (C-D) Over-expression of *cd99l2* in *cd99l2*-deficient morphants rescued the defective phenotype.

405 (E) Statistics for A-D; The 'N' represents the number of experimental animals in the statistics.

(F-G) Induced over-expression of *cd99l2* in *cd99l2*-deficient morphants rescued the defective phenotype.

(H) Representative images following the injection of dye-labeled dextran into Control MO and *cd99l2* MO erythrocytes.

(I-I') Parabiosis was observed between Control MO and *cd99l2* MO erythrocytes.

(J-K) Representative images showing *fli1a*: eGFP and globin: DsRed staining in Control MO and *cd99l2* MO erythrocytes.

(L-O) Transmission electron microscopy (TEM) observes the spatial position and morphology between erythrocytes and vessels in Control MO and *cd99l2* MO.

**** indicate $P < 0.0001$

Scale bar: 5 μm (M), 25 μm (H, K), and 200 μm (B, D, G and I).

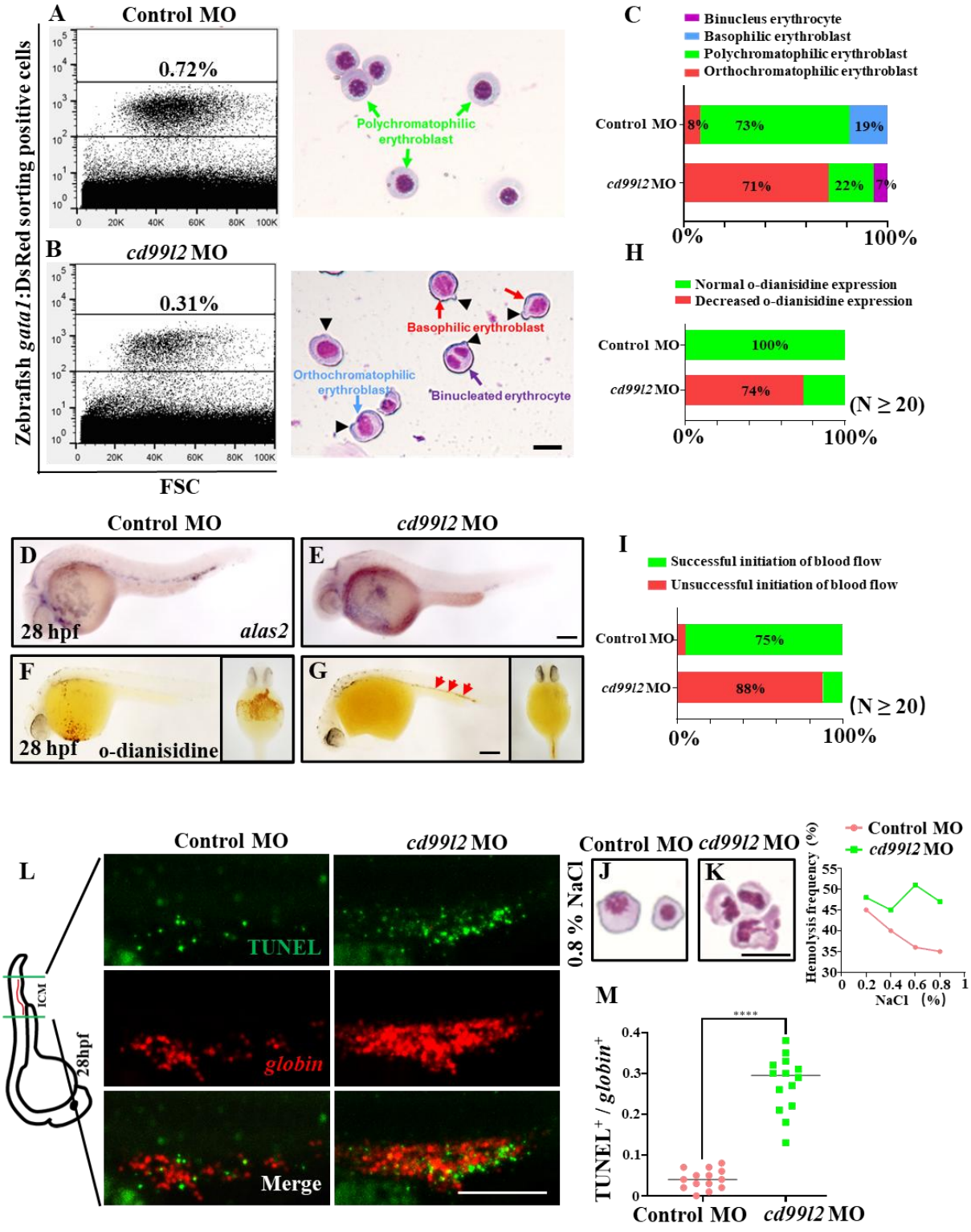

FIGURE 3. DISRUPTION OF CD99L2 LEADS TO ERYTHROCYTE MATURATION DEFECTS AND HEMOLYTIC ANEMIA IN ZEBRAFISH

(A-B) Representative images showing Giemsa staining of *gata1*-labeled erythrocytes in Control MO and *cd99l2* MO erythrocytes.

(C) Statistics for A-B.

(D-E) WISH was used to detect *alas2* expression in Control MO and *cd99l2* MO erythrocytes.

(F-G) O-dianisidine staining of Control MO and *cd99l2* MO erythrocyte.

(H) Statistics for D-E; The 'N' represents the number of experimental animals in the statistics.

(I) Statistics for F-G; The 'N' represents the number of experimental animals in the statistics.

(J-K) An osmotic fragility test was carried out in Control MO and *cd99l2* MO erythrocytes.

(L) TUNEL staining was used to examine apoptosis in Control MO and *cd99l2* MO erythrocytes.

(M) Statistics for L.

**** indicate $P < 0.001$

Scale bar: 10 μm (B, K), 100 μm (L) and 200 μm (E, G).

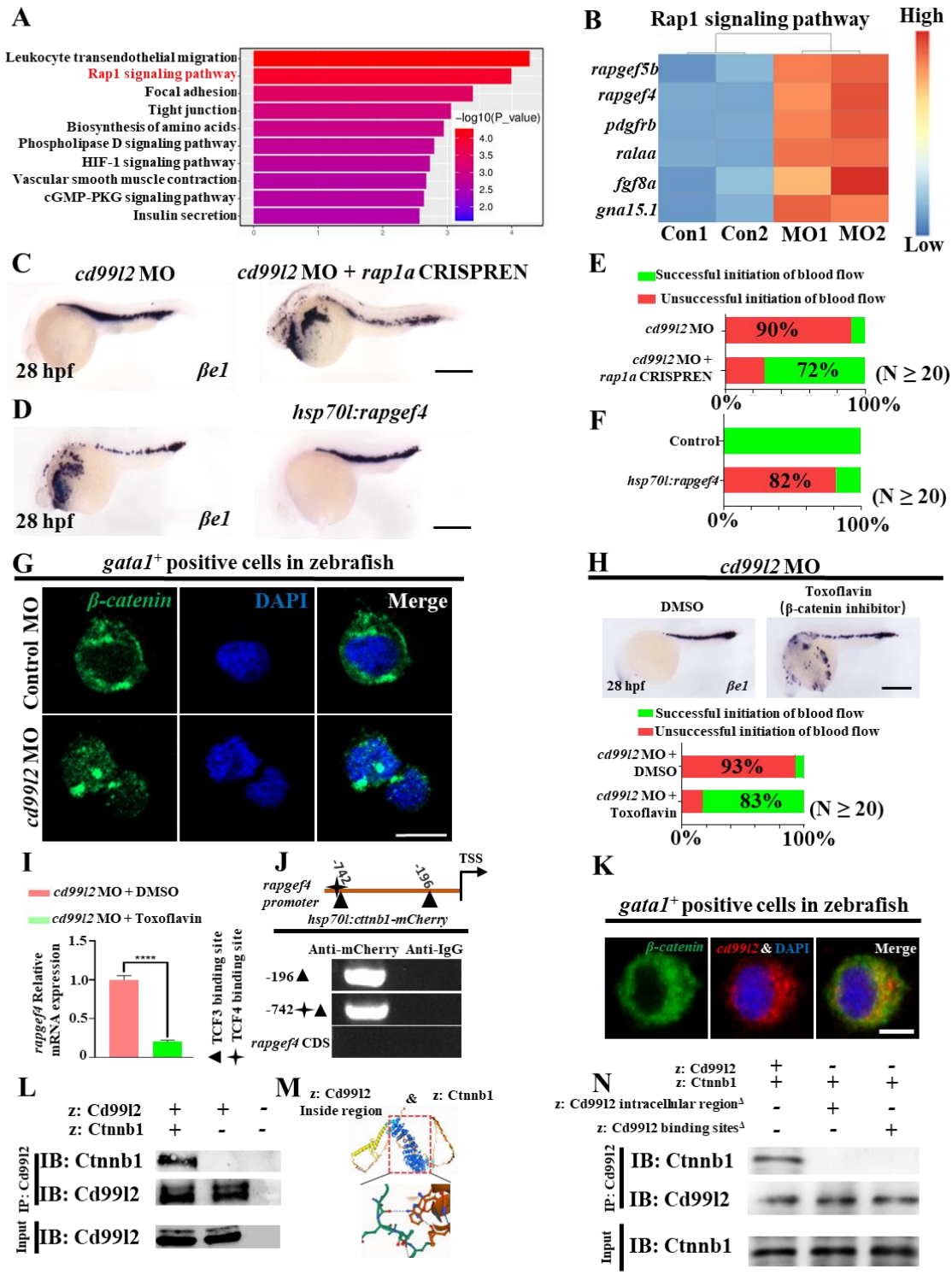

FIGURE 4. ABNORMAL ERYTHROPOIESIS IN ZEBRAFISH IS CAUSED BY ACTIVATION OF THE RAP1 SIGNALING PATHWAY AND THE TRANSLOCATION OF B-CATENIN

(A) KEGG enrichment analysis of differentially activated pathways between Control MO and *cd99l2* MO erythrocytes.

(B) Expression of genes associated with the Rap1 signaling pathway in Control MO and *cd99l2* MO erythrocytes.

(C) WISH detected *βe1* expression in *cd99l2* MO and *cd99l2* MO erythrocytes treated with *rap1a* guide RNA and Cas9 protein.

(D) WISH detected *βe1* expression in control and overexpression of *rapgef4*.

(E) Statistics for C; The 'N' represents the number of experimental animals in the statistics.

(F) Statistics for D; The 'N' represents the number of experimental animals in the statistics.

(G) Immunofluorescence staining of β-catenin in Control MO and *cd99l2* MO *gata1* labeled erythrocytes. Nucleus are stained with DAPI.

(H) WISH detected *βe1* in *cd99l2* MO treated with DMSO and β-catenin inhibitor; The 'N' represents the number of experimental animals in the statistics.

(I) qRT-PCR was used to detect the expression of *rapgef4* in *cd99l2* MO erythrocytes treated with DMSO and β-catenin inhibitor.

(J) Schematic diagram of the *rapgef4* promoter region. The transcription starting site is designated as TSS. ChIP-PCR shows that TCF3 and TCF4 bind to the promoter region of the *rapgef4* promoters.

(K) Immunofluorescence staining of *cd99l2* and β-catenin in *gata1* labeled erythrocytes, Nuclei was stained with DAPI.

(L) Co-immunoprecipitation experiment detected the interaction between *cd99l2* and β-catenin.

(M) Binding sites between *cd99l2* and β-catenin predicted by Alphafold2.

(N) Co-immunoprecipitation experiment detected the interaction between inside region deleted *cd99l2*, predicted binding sites deleted *cd99l2* and β-catenin.

**** indicate $P < 0.001$

Scale bar: 10 μm (G, K) and 200 μm (C, D, H).

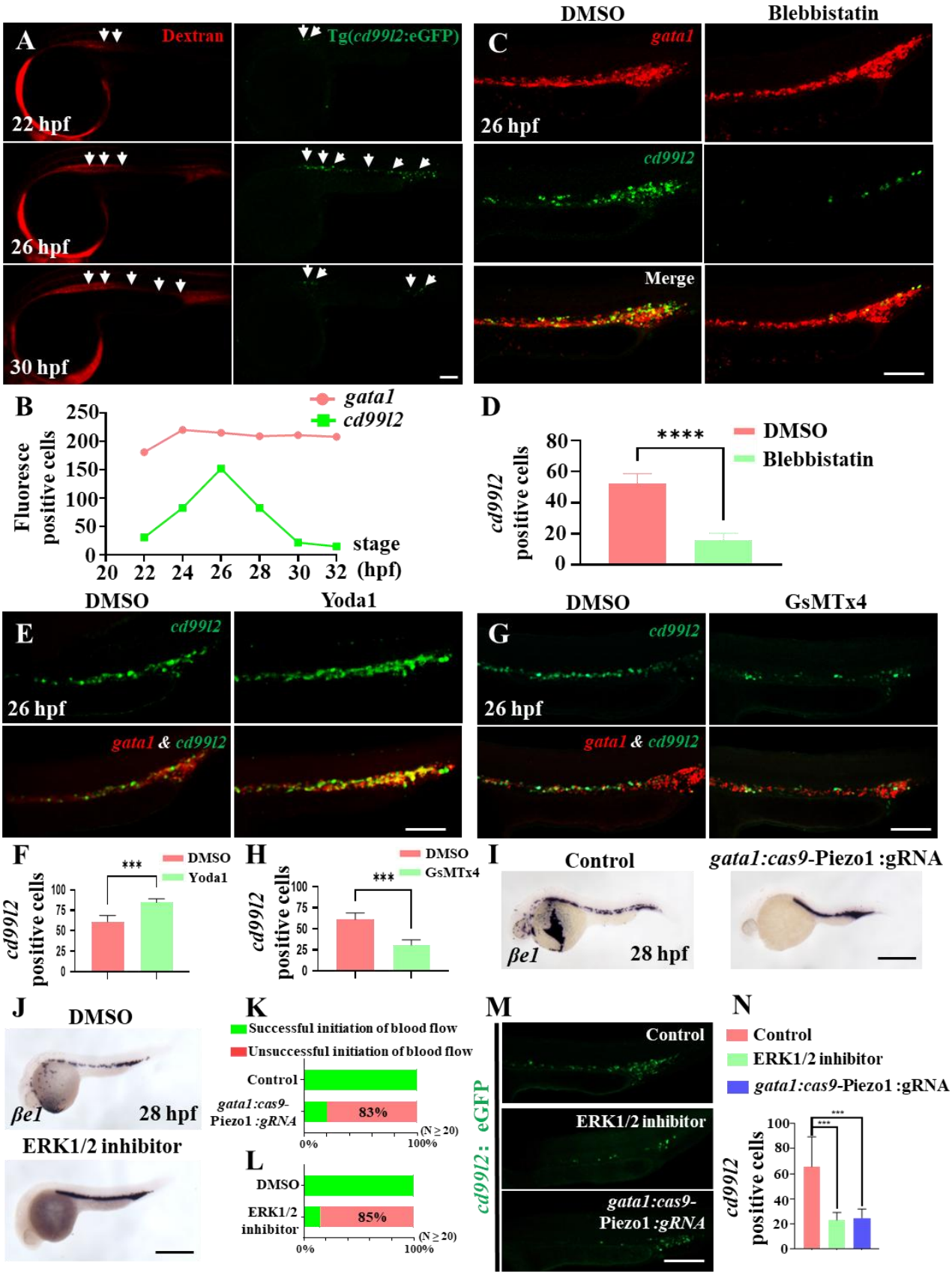

FIGURE 5. THE ACTIVATION OF PIEZO1 AND CALCIUM CHANNELS INDUCES THE EXPRESSION OF CD99L2

(A) Representative images showing *cd99l2* fluorescence after Dextran injection in zebrafish.

(B) Statistics for A.

(C) Representative images showing *cd99l2*: eGFP and *gata1*: DsRed staining in DMSO and Blebbistatin treated zebrafish.

(D) Statistics for C.

(E) Representative images showing *cd99l2*: eGFP and *gata1*: DsRed staining in DMSO and Yoda1 treated zebrafish.

(F) Statistics for E.

(G) Representative images showing *cd99l2*: eGFP and *gata1*: DsRed staining in DMSO and GsMTx4 treated zebrafish.

(H) Statistics for G.

(I) WISH detected *βe1* expression in control and embryos treated with *gata1* promoter: *piezo1* guide RNA and Cas9 protein.

(J) WISH detected *βe1* in embryos treated with DMSO and ERK1/2 inhibitor.

(K) Statistics for I; The 'N' represents the number of experimental animals in the statistics.

(L) Statistics for J; The 'N' represents the number of experimental animals in the statistics.

(M) Representative images showing *cd99l2*: eGFP in control, ERK1/2 inhibitor and *gata1* promoter: *piezo1* guide RNA with Cas9 protein treated zebrafish.

(N) Statistics for M.

**** indicate $P < 0.001$

Scale bar: 100 μm (A, C, E, G, M) and 200 μm (I, J).

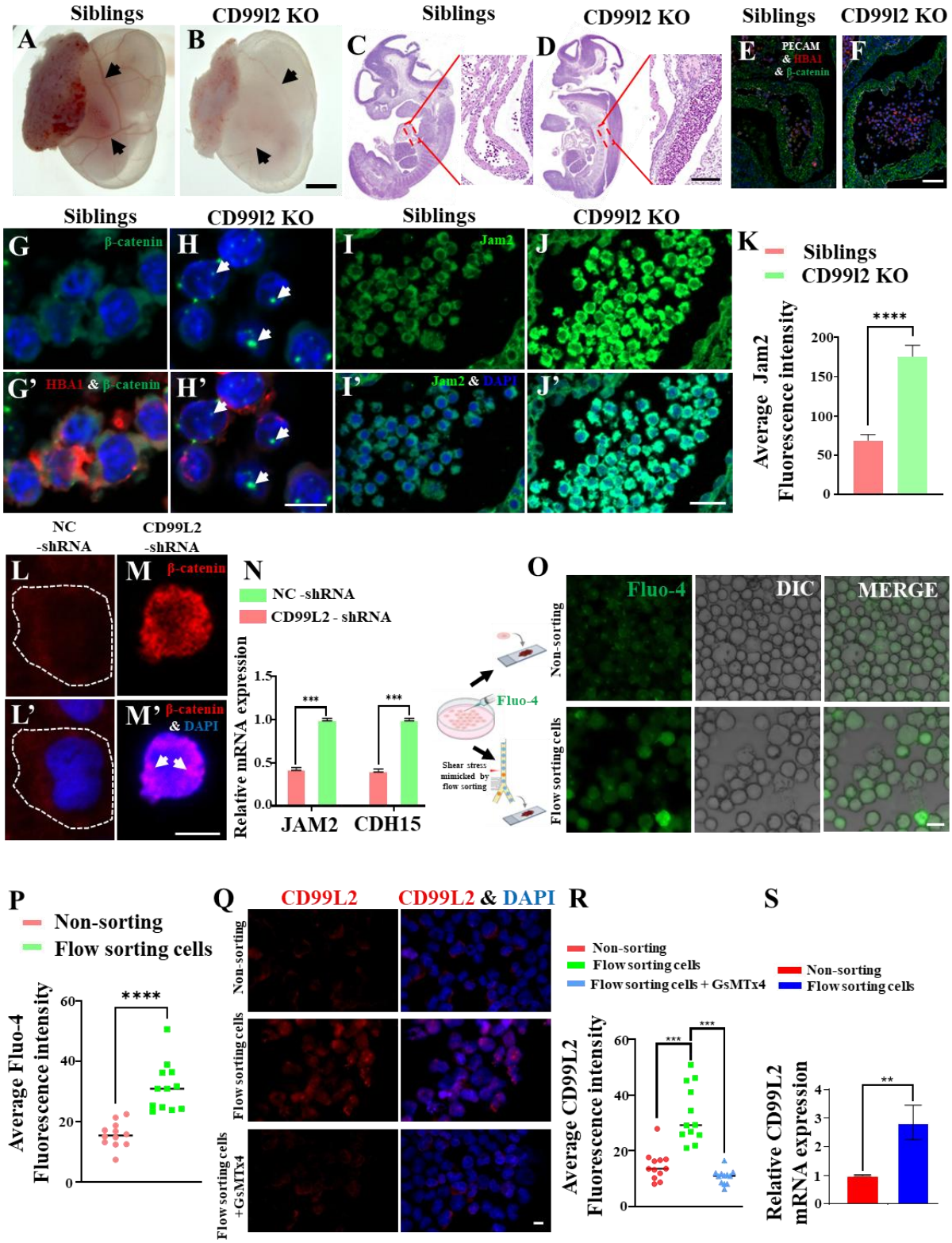

FIGURE 6. CONSERVATION VALIDATION OF THE ROLES OF CD99L2, PIEZO1, AND CALCIUM ACTIVATION IN THE INITIATION OF BLOOD FLOW

(A-B) Representative images of yolk sac from the CD99l2 knockout mice and siblings.

(C-D) H&E staining of CD99l2 knockout mice and siblings.

(E-F) Immunofluorescence staining of Siblings and CD99l2 knockout embryos sections.

(G-H) Immunofluorescence staining of β-catenin and HBA1 in Siblings and CD99l2 knockout embryos sections.

(I-J) Immunofluorescence staining of Jam2 in Siblings and CD99l2 knockout embryos sections.

(K) Statistics for I-J.

(L-M) Immunofluorescence staining of U2-OS cell lines under NC-shRNA and CD99L2-shRNA.

(N) qRT-PCR was used to detect the expression of JAM2 and CDH15 in U2-OS cell lines under NC-shRNA and CD99L2-shRNA.

(O) Detection of Fluo-4-labeled Ca^{2+} signals in K562 cells after flow cytometry sorting.

(P) Statistics for O.

(Q) Immunofluorescence staining of CD99L2, Nuclei was stained with DAPI.

(R) Statistics for Q.

(S) qRT-PCR was used to detect the expression of CD99L2.

Scale bar: 10 μm (H, M, Q), 20 μm (J, O), 50 μm (F), 100 μm (D) and 1000 μm (B).

REFERENCES

1. Montero-Balaguer, M., et al., Stable vascular connections and remodeling require full expression of VE-cadherin in zebrafish embryos. PLoS One, 2009. 4(6): p. e5772.
2. Strilić, B., et al., The molecular basis of vascular lumen formation in the developing mouse aorta. Dev Cell, 2009. 17(4): p. 505-15.
3. Iida, A., et al., Metalloprotease-dependent onset of blood circulation in zebrafish. Curr Biol, 2010. 20(12): p. 1110-6.
4. Nishii, K. and Y. Shibata, Mode and determination of the initial contraction stage in the mouse embryo heart. Anat Embryol (Berl), 2006. 211(2): p. 95-100.
5. Jones, E.A., The initiation of blood flow and flow induced events in early vascular development. Semin Cell Dev Biol, 2011. 22(9): p. 1028-35.
6. Palis, J., et al., Development of erythroid and myeloid progenitors in the yolk sac and embryo proper of the mouse. Development, 1999. 126(22): p. 5073-84.
7. Wong, P.M., et al., Properties of the earliest clonogenic hemopoietic precursors to appear in the developing murine yolk sac. Proc Natl Acad Sci U S A, 1986. 83(11): p. 3851-4.
8. Isern, J., et al., Single-lineage transcriptome analysis reveals key regulatory pathways in primitive erythroid progenitors in the mouse embryo. Blood, 2011. 117(18): p. 4924-34.
9. Ji, R.P., et al., Onset of cardiac function during early mouse embryogenesis coincides with entry of primitive erythroblasts into the embryo proper. Circ Res, 2003. 92(2): p. 133-5.
10. Kim, K., et al., Polycystin 1 is required for the structural integrity of blood vessels. Proc Natl Acad Sci U S A, 2000. 97(4): p. 1731-6.
11. Butler, P.J., et al., Shear stress induces a time- and position-dependent increase in endothelial cell membrane fluidity. Am J Physiol Cell Physiol, 2001. 280(4): p. C962-9.
12. Hanspal, M., Importance of cell-cell interactions in regulation of erythropoiesis. Curr Opin Hematol, 1997. 4(2): p. 142-7.
13. Ema, M., et al., Primitive erythropoiesis from mesodermal precursors expressing VE-cadherin, PECAM-1, Tie2, endoglin, and CD34 in the mouse embryo. Blood, 2006. 108(13): p. 4018-24.
14. Verfaillie, C.M., et al., Adhesion of committed human hematopoietic progenitors to synthetic peptides from the C-terminal heparin-binding domain of fibronectin: cooperation between the integrin alpha 4 beta 1 and the CD44 adhesion receptor. Blood, 1994. 84(6): p. 1802-11.
15. Telen, M.J., Erythrocyte adhesion receptors: blood group antigens and related molecules. Transfus Med Rev, 2005. 19(1): p. 32-44.
16. Grossin, N., M.P. Wautier, and J.L. Wautier, Red blood cell adhesion in diabetes mellitus is mediated by advanced glycation end product receptor and is modulated by nitric oxide. Biorheology, 2009. 46(1): p. 63-72.
17. Smith, J.D., et al., Malaria's deadly grip: cytoadhesion of Plasmodium falciparum-infected erythrocytes. Cell Microbiol, 2013. 15(12): p. 1976-83.
18. Papageorgiou, D.P., et al., Simultaneous polymerization and adhesion under hypoxia in sickle cell disease. Proc Natl Acad Sci U S A, 2018. 115(38): p. 9473-9478.
19. Rooks, H., et al., A gain of function variant in PIEZO1 (E756del) and sickle cell disease. Haematologica, 2019. 104(3): p. e91-e93.
20. Pijuan-Sala, B., et al., A single-cell molecular map of mouse gastrulation and early organogenesis. Nature, 2019. 566(7745): p. 490-495.
21. Colin, Y., C. Le Van Kim, and W. El Nemer, Red cell adhesion in human diseases. Curr Opin Hematol, 2014. 21(3): p. 186-92.

551 22. Steeber, D.A. and T.F. Tedder, Adhesion molecule cascades direct lymphocyte recirculation and
552 leukocyte migration during inflammation. Immunol Res, 2000. 22(2-3): p. 299-317.

553 23. McGrath, K.E., et al., Circulation is established in a stepwise pattern in the mammalian embryo.
554 Blood, 2003. 101(5): p. 1669-1675.

555 24. Samus, M., et al., CD99L2 deficiency inhibits leukocyte entry into the central nervous system and
556 ameliorates neuroinflammation. J Leukoc Biol, 2018. 104(4): p. 787-797.

557 25. Rutledge, N.S., et al., CD99-like 2 (CD99L2)-deficient mice are defective in the acute
558 inflammatory response. Exp Mol Pathol, 2015. 99(3): p. 455-9.

559 26. El Nemer, W., et al., The Lutheran blood group glycoproteins, the erythroid receptors for laminin,
560 are adhesion molecules. J Biol Chem, 1998. 273(27): p. 16686-93.

561 27. Cartron, J.P. and J. Elion, Erythroid adhesion molecules in sickle cell disease: effect of
562 hydroxyurea. Transfus Clin Biol, 2008. 15(1-2): p. 39-50.

563 28. Blum, Y., et al., Complex cell rearrangements during intersegmental vessel sprouting and vessel
564 fusion in the zebrafish embryo. Dev Biol, 2008. 316(2): p. 312-22.

565 29. El-Brolosy, M.A., et al., Genetic compensation triggered by mutant mRNA degradation. Nature,
566 2019. 568(7751): p. 193-197.

567 30. Ma, Z., et al., PTC-bearing mRNA elicits a genetic compensation response via Upf3a and
568 COMPASS components. Nature, 2019. 568(7751): p. 259-263.

569 31. Hilbi, H. and A. Kortholt, Role of the small GTPase Rap1 in signal transduction, cell dynamics and
570 bacterial infection. Small GTPases, 2019. 10(5): p. 336-342.

571 32. Jaśkiewicz, A., B. Pająk, and A. Orzechowski, The Many Faces of Rap1 GTPase. Int J Mol Sci,
572 2018. 19(10).

573 33. Goto, M., et al., Rap1 stabilizes beta-catenin and enhances beta-catenin-dependent transcription
574 and invasion in squamous cell carcinoma of the head and neck. Clin Cancer Res, 2010. 16(1): p. 65-
575 76.

576 34. Asuri, S., et al., E-cadherin dis-engagement activates the Rap1 GTPase. J Cell Biochem, 2008.
577 105(4): p. 1027-37.

578 35. Zi, H., et al., Piezo1-dependent regulation of pericyte proliferation by blood flow during brain
579 vascular development. Cell Rep, 2024. 43(1): p. 113652.

580 36. Petkova-Kirova, P., et al., The Gárdos Channel and Piezo1 Revisited: Comparison between
581 Reticulocytes and Mature Red Blood Cells. Int J Mol Sci, 2024. 25(3).

582 37. Caulier, A., et al., PIEZO1 activation delays erythroid differentiation of normal and hereditary
583 xerocytosis-derived human progenitor cells. Haematologica, 2020. 105(3): p. 610-622.

584 38. Pruszak, J., et al., Markers and methods for cell sorting of human embryonic stem cell-derived
585 neural cell populations. Stem Cells, 2007. 25(9): p. 2257-68.

586

STAR★METHODS

KEY RESOURCES TABLE

REAGENT or RESOURCE	SOURCE	IDENTIFIER
Antibodies		
Rabbit anti-DsRed	Abcam	ab62341
JAM-B Rabbit Polyclonal Antibody	Huabio	ER65451
Rabbit-anti-β-catenin	Abcam	ab227499
Alexa Fluor 488-conjugated anti-goat	Invitrogen	A32731
Alexa Fluor® 488 Rabbit	Abcam	ab199091
CD99L2 Rabbit pAb	Abclonal	A15097
Fluo-4, AM, Cell Permeant	YEASON	40704ES50
Chemicals, peptides, and recombinant proteins		
Toxoflavin	MCE	HY-100760
DMSO	Sigma–Aldrich	D8418
Sulforaphene (erk inhibitor)	MCE	HY-N2450
Borussertib （AKT inhibitor）	MCE	HY-122913
BD750 (STAT5 inhibitor)	MCE	HY-131140
Verteporfin (Yap inhibitor)	MCE	HY-B0146
Deposited data		
https://kleintools.hms.harvard.edu/paper_websites/tusi_et_al/	PMID: 29466336	mouse blood cell singlecell RNAseq
Experimental models: Cell lines		
K562	Cell Bank/Stem Cell Bank of the Chinese Academy of Sciences	RRID: CVCL_0004
U2OS	Cell Bank/Stem Cell Bank of the Chinese Academy of Sciences	RRID: CVCL_0042
RNA-seq data	NCBI	PRJNA1426740
Experimental models: Organisms/strains		
Tg(gata1:DsRed)	PMID: 14608381	Erythrocyte progenitor cell marker transgenic zebrafish
Tg(globin:DsRed)	PMID: 29229770	Erythrocytes marker transgenic zebrafish
Tg(fli1a:eGFP)	PMID: 12167406	Blood vessel marker transgenic zebrafish
Tg(coro1a:eGFP)	PMID: 19168679	Myeloid cells marker transgenic zebrafish
Tg(rag2:DsRed)	PMID: 9089097	Lymphoid cells marker transgenic zebrafish
C57BL/6J	model organism (CHINA)	wild type
C57BL/6J-^{Cd99l2em1Smoc}	model organism (CHINA)	CD99L2 MUTANT MOUSE
Oligonucleotides		
zebrafish:cd99l2 mrna (WISH probe)	FP:TGCTGGTAGTGAAAGGCTTGAGTGATGG RP:GAGTTTGTTGAACTTGTGGCTCCTGTGC	Designed based on Ensembl
zebrafish:cd99l2 qPCR (qPCR)	FP ： CTACGACACCATGGCTGAGACT RP:CTTGTGGCTCCTGTGCGACTAC	Designed based on Ensembl
zebrafish:ef-1α (qPCR)	FP:TACTTCTCAGGCTGACTGTG RP:ATCTTCTTGATGTATGCGCT	Designed based on Ensembl
zebrafish:cd99l2 promoter (promoter clone)	FP:acgcGTCGACCAGCCGCTGAGCATGTTCTTGAC RP:tgACCGGTGTCCATGTCCAGAGCGTCTTCT	Designed based on Ensembl
zebrafish:cd99l2 cds (MO rescue)	FP:ATGGAGAAGACGCTCTGGACAT RP:AACTGCATTTTCTTCTGTTGGTGGC	Designed based on Ensembl
human:cd99l2 qPCR (qPCR)	fp:CAGACTACGTGAAGGGAGAGA rp:TTGGGGTTCCTCACATACCAC	Designed based on Ensembl
human:CDH15 qPCR (qPCR)	fp:TCCCAGGCACCTATGTGAC rp:CTTGCACTGTGCGGATCTCTC	Designed based on Ensembl

human:JAM2 qPCR (qPCR)	fp:AACTGGGTCGGAGTGTCTC rp:GGGGCACTAACTTCACAACGA	Designed based on Ensembl
piezo1 cas9 target1	TGATGTGTGCCTCTCAGCAG	Reference （PMID: 38175750）
piezo1 cas9 target2	GAAGAGTGGATGGTCATGGG	Reference （PMID: 38175750）
piezo1 cas9 target3	GCTCAGTGTGGTCAACCCGG	

METHOD DETAILS

Animals and ethical husbandry

Zebrafish experiments were conducted according to the guidelines of the Institutional Animal Care and Use Committee of South China University of Technology. Zebrafish were bred under standard conditions (28.5°C, 14-h light; 10-h dark) in a standard circulating water system[38]. The following strains were used: AB strain, Tg (*gata1*: DsRed)[39], Tg (*globin*: DsRed)[40], Tg (*fli1a*: eGFP)[41], Tg (*coro1a*: eGFP)[42], and Tg(*rag2*: DsRed)[43].

The knockout strategy and technical routes of the CD99L2-KO mice are detailed on the official website (https://www.modelorg.com/portal/search/index.html?keyword=CD99L2). The mice acclimated under standard laboratory conditions (25 ℃ ± 1 ℃, 60% ± 5% humidity,12-h light/dark cycle).

All experiments were conducted in accordance with the Guiding Principles in the Care and Use of Animals (China) and were approved by the Laboratory Animal Ethics Committee of South China University of Technology (approval number AE-2026017).

Cell culture

293T (RRID: CVCL_0063), U2OS (RRID: CVCL_0042), and K562 (RRID: CVCL_0004) cells were obtained from the Cell Bank/Stem Cell Bank of the Chinese Academy of Sciences. Cells were cultured in DMEM medium (Gibco 12,491,015) containing 10% FBS (Gibco 10,270,106) and placed at 37°C with 5% CO^2.

Single-cell gene expression analysis

The expression profiles of various adhesion molecules in mouse erythrocytes were obtained from a publicly available single-cell database https://kleintools.hms.harvard.edu/paper_websites/tusi_et_al/[44].

In vitro synthesis of antisense RNA probes and mRNA

Antisense digoxigenin (DIG)-labeled RNA probes (Roche Applied Science, Basel, Switzerland) were synthesized using an in vitro transcription reaction following standard protocols[38]. Capped mRNA was prepared using the mMachine® sp6 kit according to the manufacturer's instructions.

Whole-mount in situ hybridization (WISH)

DIG-labeled RNA probes were transcribed with T7, T3, or SP6 polymerase (Ambion, Life Technologies, USA). WISH was performed as previously described[45]. DIG-labeled probes were detected using anti-DIG Fab fragment antibody (Roche Applied Science) with BCIP/NBT staining (Vector Laboratories, Burlingame, CA, USA).

Immunostaining

Embryos were collected and fixed overnight at 4 ℃ with 4% paraformaldehyde, then permeabilized with methanol. Residual methanol was rinsed and washed by PBST (PBS containing 0.1% Tween-20). After blocking with blocking buffer (0.5% Triton-X PBS, 5% lamb serum, and 1% DMSO) for 2 h at room temperature, embryos were incubated with primary antibody in blocking buffer for 1 day, followed by secondary antibody for another day at 4 ℃. The primary antibodies and secondary antibodies used are listed in STAR METHODS (KEY RESOURCES TABLE).

Confocal imaging

Zebrafish embryos were mounted in 1% low-melting agarose with 0.01% tricaine. A Zeiss 800 confocal microscope was used for imaging the samples. A 561-nm laser with an emission wave length range of 570–650 nm and a 488-nm laser with an emission wave length range of 500–550 nm were utilized. The microscope was operated on the Zeiss Zen blue 2.5 software platform (Carl Zeiss).

Fluorescence-activated cell sorting (FACS)

Flow cytometry was used to sort purified hematopoietic cells from transgenic embryos at the desired stage as described previously[46] using a flow cytometer (Becton Dickinson, San Jose, CA, USA). Data were analyzed using FlowJo software (TreeStar, Ashland, OR, USA).

RNA extraction and quantitative RT-PCR

Total RNA was extracted from sorted cells using TRIzol Reagent (Roche Applied Science) following the manufacturer's instructions, then reverse transcribed into complementary DNA (cDNA) using M-MLV Reverse Transcriptase (Promega, Madison, USA) with oligo-dT (deoxy-thymine) primers. RNA was treated with RNase-free DNase (Thermo Fisher Scientific, Waltham, USA) before the reverse transcription reaction. qRT-PCR reactions were performed using the LightCycler Nano System (Roche Applied Science) with FastStart Universal SYBR Green Master (ROX) (Roche Applied Science) and 10 pmol of each primer. Each sample was tested in triplicate. The housekeeping gene, elongation factor 1-α (ef-1α), served as an internal control to normalize the relative fold changes using the Δ Δ Ct threshold method. The primers used are listed in STAR METHODS (KEY RESOURCES TABLE).

Vector construction and generation of transgenic line

A 4.7-kb DNA fragment upstream of the *cd99l2* translation start site was isolated to drive GFP expression in the Tol2 vector. The pTol2-*cd99l2*-eGFP construct was injected into one-cell stage embryos to generate transgenic lines. The primers used are listed in STAR METHODS (KEY RESOURCES TABLE).

May-Grünwald Giemsa staining of transgenic blood cells

Blood cells were collected in PBS containing 10% FBS, then cytospun onto slides by centrifugation at 450 rpm for 3 min using a Cytospin 4 (Thermo Scientific). The slides were then air-dried and subjected to May-Grünwald Giemsa staining according to the standard protocol.

MO injection

The following MO sequence was used: 5'-AACTGGGTTGCTGCGATATTAAATA-3', while the standard control MO was purchased from Gene Tools. One-cell stage embryos were injected with 2 nl of MO solution at a concentration of 0.8 mM.

Parabiosis experiment

The parabiosis experiment was performed as described previously[47,48]. Briefly, control MO and *cd99l2* MO embryos were dechorionated at approximately 3 hpf and transferred into a 4% methylcellulose drop under HCR solution (166 mM NaCl, 2.9 mM KCl, 10 mM CaCl2, and 5 mM HEPES in egg water). The embryos were repositioned using a gel-loading pipet so that their animal poles were in direct contact with each other. A few cells were detached from each embryo, and the wounded tissues of each embryo were properly aligned until they fused together.

Osmotic fragility assay

The osmotic fragility assay was performed after the parabiosis experiment as previously described[49]. Freshly drawn blood from wild-type and homozygous adult fish was washed three times in 0.9% NaCl and suspended in saline to approximately 10% packed cell volume. A cell suspension (5 ml) was added to each of 150 ml solutions containing NaCl concentrations ranging from 0.200% to 0.900% (wt/vol). The cells were incubated at room temperature for 15 min, then centrifuged for 3 min at 420 g.

TUNEL staining

TUNEL staining was performed with an In Situ Cell Death Detection Kit (#11684795910, Roche) as previously described[50].

RNA-Seq and Bioinformatic Analysis

The RNA was extracted with TRIzol reagent (Invitrogen, CA,United States; 15596026) and sequencing libraries were generated using the NEBNext® UltraTM RNA Library Prep Kit for Illumina® RNA (NEB; E7770) according to the manufacturer's instructions. For RNA-seq data, the sequencing reads were mapped to Ensemble zebrafish reference genome (GRCz11) using STAR alignment software[51]. The differential gene expression analysis was performed by DESeq2[52]. For GO and KEGG enrichment analysis, the Kobas website (http://bioinfo.org/kobas) was used[53].

Drug exposure

Zebrafish embryos at 22 hpf were soaked in egg water containing chemicals for at 6 hours, and relevant experiments were performed at 28 hpf. DMSO, Toxoflavin, Sulforaphene, Borussertib, BD750, Verteporfin were used in this study.

Western blotting

The zebrafish embryos and cells were dissected and lysed in RIPA lysis buffer supplemented with protease inhibitor cocktail (Roche, #04693116001) for Western blot analysis. The proteins were then separated by One-Step PAGE Gel Fast Preparation Kit (Vazyme, # E303-01) and transferred to nitrocellulose (NC) membranes. Membranes were first blocked in 5% skimmed milk powder in TBST and then incubated overnight at 4°C with primary antibodies. Subsequently, the membranes were incubated with secondary antibodies for another 2h. Images were visualized with a MiniChemi image system (Beijing Sage Creation Science Co., China). All the information on primary antibodies is listed in STAR METHODS (KEY RESOURCES TABLE).

Erythrocytes-specific *piezo1* disruption in zebrafish

The erythrocytes-specific *piezo1* CRISPR vector was constructed as previously described[54].In briefly, it takes advantage of the Tol2 transposase technology to integrate in the zebrafish genome a vector expressing a guide RNA (gRNA) from a zebrafish U6 promoter and Cas9 under the control of a tissue-

specific promoter. The primer for *piezo1* Cas9 target is listed in STAR METHODS (KEY RESOURCES TABLE).

Co-immunoprecipitation

The plasmids carrying hsp70l-*cd99l2*-eGFP and hsp70l-*ctnnb1*-mCherry are constructed. The embryos undergo multiple heat shock treatments at 24-30 hpf to induce the expression of heatshock-driven proteins. Following heat shock, the embryos are collected, and total protein is extracted. The 10% of the total protein is reserved as the "Input". The “Input” samples are analyzed using antibodies against GFP and mCherry to detect the expression of the respective fusion proteins. The remaining protein is incubated overnight with anti-GFP antibodies to immunoprecipitate the Cd99l2-eGFP fusion protein and any potential interacting partners. The bound proteins (including Cd99l2-eGFP and any potential interacting partners) are subjected to Western blot analysis using both anti-GFP and anti-mCherry antibodies.

Statistical analysis

Statistical analyses were conducted using GraphPad Prism 8 (GraphPad Software Inc., San Diego, CA) software. Sample sizes (n) was provided in the text or figure legend for each experiment and each experiment was independently repeated at least three times. The significance of differences between two groups was calculated using the two-tailed Student’s t-test. The chi-square test was used to compare whether there were significant differences in subtyped variables between the two groups. Error bars represent the mean ± standard error in all graphs. A P value less than 0.05 was considered significant. The densities of the western blot bands were analyzed by ImageJ software

REFERENCES

39. Westerfield, M. The zebrafish book : a guide for the laboratory use of zebrafish (Danio rerio). 1995.

40. Traver, D., et al., Transplantation and in vivo imaging of multilineage engraftment in zebrafish bloodless mutants. Nat Immunol, 2003. 4(12): p. 1238-46.

41. Zhang, Z., et al., Retinoblastoma 1 protects T cell maturation from premature apoptosis by inhibiting E2F1. Development, 2018. 145(1).

42. Lawson, N.D. and B.M. Weinstein, In vivo imaging of embryonic vascular development using transgenic zebrafish. Dev Biol, 2002. 248(2): p. 307-18.

43. Jin, H., et al., Definitive hematopoietic stem/progenitor cells manifest distinct differentiation output in the zebrafish VDA and PBI. Development, 2009. 136(4): p. 647-54.

44. Willett, C.E., J.J. Cherry, and L.A. Steiner, Characterization and expression of the recombination activating genes (rag1 and rag2) of zebrafish. Immunogenetics, 1997. 45(6): p. 394-404.

45. Tusi, B.K., et al., Population snapshots predict early haematopoietic and erythroid hierarchies. Nature, 2018. 555(7694): p. 54-60.

46. Thisse, C. and B. Thisse, High-resolution in situ hybridization to whole-mount zebrafish embryos. Nat Protoc, 2008. 3(1): p. 59-69.

47. Manoli, M. and W. Driever, Fluorescence-activated cell sorting (FACS) of fluorescently tagged cells from zebrafish larvae for RNA isolation. Cold Spring Harb Protoc, 2012. 2012(8).

48. Hagedorn, E.J., et al., Generation of Parabiotic Zebrafish Embryos by Surgical Fusion of Developing Blastulae. J Vis Exp, 2016(112).

49. Ding, Y., et al., The chromatin-remodeling enzyme Smarca5 regulates erythrocyte aggregation via Keap1-Nrf2 signaling. Elife, 2021. 10.

761 50. Shafizadeh, E., et al., Characterization of zebrafish merlot/chablis as non-mammalian vertebrate
762 models for severe congenital anemia due to protein 4.1 deficiency. Development, 2002. 129(18): p.
763 4359-70.

764 51. Li, X., et al., SUMO1-activating enzyme subunit 1 is essential for the survival of hematopoietic
765 stem/progenitor cells in zebrafish. Development, 2012. 139(23): p. 4321-9.

766 52. Dobin, A., et al., STAR: ultrafast universal RNA-seq aligner. Bioinformatics, 2013. 29(1): p. 15-21.

767 53. Love, M.I., W. Huber, and S. Anders, Moderated estimation of fold change and dispersion for
768 RNA-seq data with DESeq2. Genome Biol, 2014. 15(12): p. 550.

769 54. Xie, C., et al., KOBAS 2.0: a web server for annotation and identification of enriched pathways
770 and diseases. Nucleic Acids Res, 2011. 39(Web Server issue): p. W316-22.

771 55. Ablain, J., et al., A CRISPR/Cas9 vector system for tissue-specific gene disruption in zebrafish.
772 Dev Cell, 2015. 32(6): p. 756-64.

773